Catalysis Science & Technology

PAPER

View Article Online
View Journal | View Issue

Cite this: *Catal. Sci. Technol.*, 2014, 4, 1268

Effect of TiO_2 crystal structure on the catalytic performance of Co_3O_4/TiO_2 catalyst for low-temperature CO oxidation

Jie Li,[a] Guanzhong Lu,*[ab] Guisheng Wu,[b] Dongsen Mao,[b] Yanglong Guo,[a] Yanqin Wang[a] and Yun Guo[a]

Received 3rd December 2013,
Accepted 22nd January 2014

DOI: 10.1039/c3cy01004j

www.rsc.org/catalysis

Co_3O_4 catalysts supported on TiO_2 with different crystalline structures (anatase (A), rutile (R) and P25 (Degussa)) were prepared by a deposition–precipitation method, and characterized by nitrogen adsorption/desorption, XRD, HR-TEM, EPR, Raman spectroscopy, XPS and H_2-TPR techniques. The results show that Co_3O_4/TiO_2 (A) exhibited the highest activity among the three Co_3O_4/TiO_2 catalysts: CO can be completely oxidized to CO_2 at −43 °C. When rutile TiO_2 or P25 were used as the support, its catalytic activity was decreased obviously, because the TiO_2 crystal structure has an influence on the physicochemical and catalytic properties of the Co_3O_4 catalysts. The results show that the Co_3O_4/TiO_2 (A) catalyst contains Ti^{3+} species, which is in an unstable state and can affect the properties of Co_3O_4 by the interaction between the deposited Co_3O_4 and anatase TiO_2 support. The Co_3O_4/TiO_2 (A) catalyst exhibits highly defective structure and good oxygen adsorption ability. The reducibility of Co_3O_4 is improved by the anatase TiO_2 support, resulting in Co_3O_4/TiO_2 (A) possessing the better redox property than the other Co_3O_4/TiO_2 catalysts, which is an important factor for its high catalytic activity.

1. Introduction

Low-temperature oxidation of CO, as one of the most extensively studied reactions in the heterogeneous catalysis field, is becoming increasingly important in cleaning air and lowering automotive emissions.[1,2] For the catalysts for CO oxidation, the precious metals (Pd, Pt and nano-Au) are well-known catalysts with high activity,[3–6] but the reaction temperature of CO complete conversion over precious metals (such as Pt) is still pretty high and their stabilities are still poor. To overcome the high cost of precious metals, researchers try to design and develop the non-precious metal catalysts, such as the metal oxide catalysts. Among them, cobalt oxide (Co_3O_4) is thought to be a potential catalyst,[7–10] because of its high activity for CO oxidation even at below 0 °C.[11,12] Hence, Co_3O_4 catalysts for low-temperature CO oxidation are widely studied,[10,13,14] including mix-valenced CoO_x,[9] supported Co_3O_4,[12] noble metal (Au, Pt) supported on Co_3O_4,[11,12] and Fe(or Ce)-doped Co_3O_4 catalyst,[15,16] *etc.* These studies above for Co_3O_4 catalysts are mainly focused on the preparation of Co_3O_4 and foreign element doping; for supported Co_3O_4 catalysts, their catalytic activities need still to be improved and the effects of structure and physicochemical properties of support on the catalytic performance of Co_3O_4 are less studied.

Titanium oxide (TiO_2) is extensively used in solid catalysts, particularly as a catalyst support.[17–20] When nano-metal particles are supported on TiO_2, there are often a strong metal-support interaction (SMSI).[21] TiO_2 possesses multi-crystalline structures, and is mainly classified into anatase, rutile and brookite phases, among which anatase and rutile TiO_2 are generally used as engineering materials more frequently than the brookite phase TiO_2. As a photo-catalyst, TiO_2 crystalline phases can affect obviously its photo-catalytic activity.[22–24] Palladium supported on anatase TiO_2 shows a higher activity than that on rutile TiO_2 for the selective hydrogenation of long chain alkadienes, due to the superior SMSI between Pd and anatase TiO_2.[25] Nanba *et al.*[26] studied the catalytic decomposition of acrylonitrile over Ag supported on TiO_2 with different crystal phases, and found that Ag/TiO_2 containing anatase TiO_2 exhibited higher NH_3 and N_2 selectivity at low and high temperatures, whereas Ag/TiO_2 with only rutile phase exhibited medium N_2 and higher NO_x selectivity at low and high temperatures. This may suggest that different crystalline phases of the TiO_2 support can affect the SMSI,[18] electronic density, oxidation state, crystal

[a] *Key Laboratory for Advanced Materials and Research Institute of Industrial Catalysis, East China University of Science and Technology, Shanghai 200237, PR China. E-mail: gzhlu@ecust.edu.cn; Fax: +86 21 64253824*
[b] *Research Institute of Applied Catalysis, Shanghai Institute of Technology, Shanghai 200235, PR China*

size[20] and metal dispersion[27] of the deposited metal components. These changes in deposited metals (or metal oxides) supported on TiO_2 with different crystalline phases can have a dramatic impact on the catalytic performance.

Herein, we investigated mainly the effect of TiO_2 crystalline phases on the catalytic performance of Co_3O_4/TiO_2 for CO oxidation, as an approach to prepare a highly effective Co_3O_4/TiO_2 catalyst. Three kinds of TiO_2 with different crystalline structures were utilized as the supports of Co_3O_4 catalyst. We have found that Co_3O_4 supported on anatase TiO_2 (Co_3O_4/TiO_2 (A)) exhibits excellent catalytic activity and CO is completely converted at −43 °C. On the basis of the physicochemical properties of Co_3O_4/TiO_2 (A) obtained, the role of different crystalline phases of TiO_2 on promoting its catalytic activity was discussed.

2. Experimental section

2.1 Catalyst preparation

The TiO_2 supports used here are anatase phase (TiO_2 (A)), P25 and rutile phase (TiO_2 (R)) respectively. TiO_2 (A) (99.8% purity) and TiO_2 (R) (99.8% purity) were purchased from Aladdin industrial corporation. P25 contains both anatase and rutile phase and was purchased from Degussa Co.

The Co_3O_4/TiO_2 catalysts were prepared by a deposition–precipitation (DP) method. Weighed $Co(NO_3)_2{\cdot}6H_2O$ were dissolved in 100 ml de-ionized water at room temperature, and then 3 g TiO_2 (less than 100 mesh) were fully dispersed in the above solution. A sodium carbonate solution (1 M) was added to this suspension under continuous stirring until pH reached 10. This suspension was aged under stirring for 30 min and statically for 2 h, and then the precipitates were filtered, washed with de-ionized water several times, dried in air at 80 °C and calcined at 350 °C for 3 h in a muffle furnace. The synthesized catalysts are denoted as Co_3O_4/TiO_2 (A), Co_3O_4/TiO_2 (P25) and Co_3O_4/TiO_2 (R) according to the crystalline phase of the TiO_2 support. The metal oxide loading was 10 wt.% on the support.

2.2 Catalytic activity testing

The activities of the catalysts for CO oxidation were tested in a continuous flow quartz tube micro-reactor (Φ 8 mm × 23 cm). 200 mg catalyst (40–60 mesh) was packed in the middle of the reactor. The flow rate of feed gas consisted of 1% CO, 10% O_2 and 89% N_2 was 20 ml min^{-1}. Before activity testing, the catalyst was pretreated in N_2 flow at 450 °C for 30 min and then cooled down to room temperature.

2.3 Characterization of catalysts

The BET surface areas of samples were measured by N_2 adsorption/desorption at −196 °C on a micromeritics ASAP-2020 instrument, and calculated by the Brunauer–Emmett–Teller (BET) method. Powder X-ray diffraction (XRD) patterns were recorded on a PANalytical PW 3040/60 X'Pert Pro powder diffractometer with CuKα radiation, which was operated at 40 kV and 40 mA and a scanning speed was 0.5° min^{-1}. High resolution transmission electron microscopy (HR-TEM) images were obtained on a JEOL JEM-2100 microscope operated at 200 kV, and the sample to be measured was first dispersed in ethanol and then collected on a copper grids covered with carbon film. After the liquid phase was evaporated the grid was loaded into the microscope. The EPR spectra were obtained on a Bruker EMX-8/2.7 EPR Spectrometer. Laser Raman spectra of samples were obtained on a Renishaw Raman spectrometer at ambient condition and the 514 nm line of a Spectra Physics Ar^+ laser was used as an excitation. The laser beam intensity and the spectrum slit width were 2 mW and 3.5 cm^{-1}, respectively. X-ray photoelectron spectroscopy (XPS) spectra of samples were obtained on a Kratos Axis Ultra-DLD photoelectron spectrometer equipped with AlKα (1486.6 eV) radiation as the excitation source. All binding energies (BE) were determined with respect to the C 1s line (284.8 eV) originating from adventitious carbon.

H_2-Temperature programmed reduction (H_2-TPR) was performed in a quartz U-tube with 50 mg sample. After the sample was pretreated in N_2 at 450 °C for 30 min, it was cooled down to room temperature, and then the reduction gas of 10 vol.% H_2/N_2 (25 ml min^{-1}) was used instead of N_2. The heating rate was 10 °C min^{-1}. The uptake amounts of H_2 were measured by a thermal conductivity detector (TCD).

3. Results and discussion

3.1 Catalytic activity

The catalytic conversions of CO as a function of the reaction temperature over three catalysts under dry or moist conditions are shown in Fig. 1. The results show that three catalysts exhibit pretty good activity for CO oxidation under dry condition, and CO can be oxidized to CO_2 at ambient temperature. Among the three catalysts, Co_3O_4/TiO_2 (A) shows the best activity for CO oxidation, in which the reaction temperature of the CO complete conversion (T_{100}) is −43 °C. For the Co_3O_4/TiO_2 (P25) and Co_3O_4/TiO_2 (R) catalysts, their

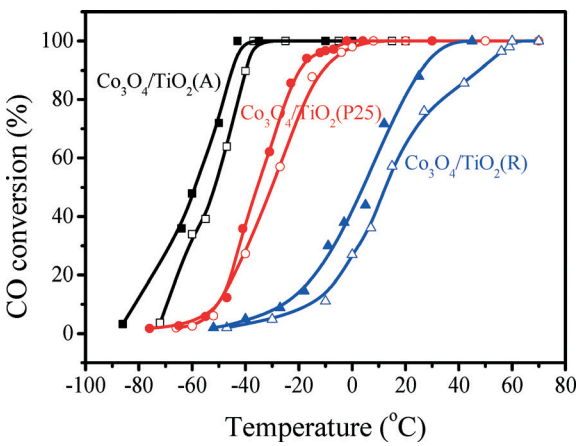

Fig. 1 The catalytic activities of Co_3O_4/TiO_2 catalyst (200 mg) for CO oxidation under dry condition (solid symbol) and 0.1% H_2O condition (hollow symbol).

T_{100} are increased to −2 °C and 45 °C respectively. Under moist condition (0.1% H_2O), the activities of the three catalysts are decreased, their T_{50} (the reaction temperature for 50% CO conversion) are raised by 6–8 °C. The reason is that water might occupy the active sites of cobalt oxide, resulting in a deactivation of the catalyst.

The stabilities of the catalysts under dry or moist condition were also tested at 15 °C. As the results in Fig. 2 show, the stability of Co_3O_4/TiO_2 (A) is the best among the three catalysts, its CO conversion can be maintained at 100% after 180 min of reaction under dry condition, and then its activity is decreased. Under moist condition, because of the poison effect of water, the activity of Co_3O_4/TiO_2 (A) is decreased much faster than that under dry condition. As for Co_3O_4/TiO_2 (P25) and Co_3O_4/TiO_2 (R), their activities are decreased as the reaction begins, and totally lost after 60 min of reaction, regardless under which (dry or moist) condition.

Even so, the results above (Fig. 1 and 2) indicate that the crystalline phase of TiO_2 support has an obvious influence on the performance of the Co_3O_4/TiO_2 catalyst for CO oxidation. As Co_3O_4/TiO_2 (R) deactivates more early than other two samples, its light-off curve shows the shallower slope than that of the other two samples, because a deactivation of the active sites on Co_3O_4/TiO_2 (R) has taken place ceaselessly when the reaction temperature rose.

3.2 N_2 adsorption–desorption and XRD

With the help of low-temperature N_2 adsorption, the BET surface areas (S_{BET}) of Co_3O_4/TiO_2 (A), Co_3O_4/TiO_2 (P25) and Co_3O_4/TiO_2 (R) were measured, and found to be 91.8 $m^2\ g^{-1}$, 48.7 $m^2\ g^{-1}$ and 38.0 $m^2\ g^{-1}$, respectively. These results illustrate that Co_3O_4 supported on the anatase TiO_2 possesses a larger BET surface area than the other two catalysts, which may be one of the reasons for its high catalytic activity for CO oxidation.

The XRD patterns of the three TiO_2 supports and three Co_3O_4/TiO_2 catalysts are shown in Fig. 3. The characteristic diffraction peaks of anatase TiO_2 were detected at 2θ = 25.4° (101), 37.9° (004) and 48.1° (200), and the diffraction peaks of rutile TiO_2 are located at 2θ = 27.5° (110), 36.1° (101) and 54.4° (211). The crystallite sizes of the supports were calculated by Sherrer's equation[28] and shown in Table 1. The results show that the crystallite size of TiO_2 (R) > TiO_2 (P25) > TiO_2 (A). In the XRD patterns of Co_3O_4 supported on different supports, the characteristic XRD peaks of Co_3O_4 cannot be observed, indicating that Co_3O_4 particles highly dispersed on the support or its particles are too small to be detected by XRD.

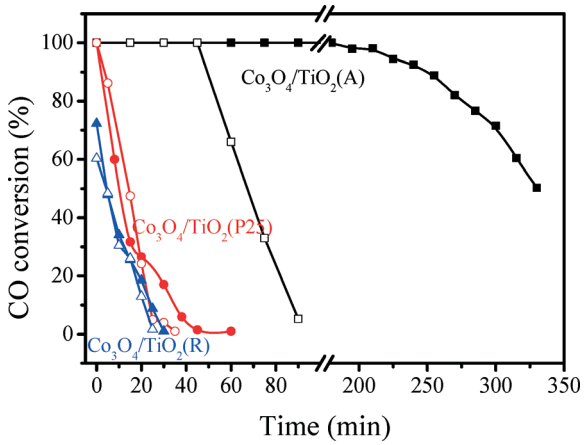

Fig. 2 The long-term stabilities of Co_3O_4/TiO_2 catalysts for CO oxidation under dry condition (solid symbol) and 0.1% H_2O condition (hollow symbol) at 15 °C.

3.3 High-resolution transmission electron microscopy (HR-TEM)

Representative HR-TEM images of Co_3O_4/TiO_2 (A), Co_3O_4/TiO_2 (P25) and Co_3O_4/TiO_2 (R) catalysts are shown in Fig. 4. The crystallite sizes of the three catalysts are 10–30 nm and the rank of the crystallite size is Co_3O_4/TiO_2 (A) > Co_3O_4/TiO_2 (P25) > Co_3O_4/TiO_2 (R), which is in agreement with the calculated results by Scherrer formula on the basis of the X-ray diffraction peak broadening. It is difficult to distinguish Co_3O_4 from TiO_2 in the TEM images. In the HR-TEM image (Fig. 4B), Co_3O_4 crystallites can be observed by the help of the ordered fingerprints with the space distance (0.243 nm) between (311) facets in the crystalline Co_3O_4 (in white rectangle). The TiO_2 crystallites which were shown in the white circle can be distinguished by the space distance (0.352 nm) between (101) facets in the crystalline anatase TiO_2.

3.4 Electron paramagnetic resonance (EPR)

EPR is a useful technique for obtaining information on the electronic structure of solid catalysts. The EPR spectra of Co_3O_4/TiO_2 catalysts are shown in Fig. 5A, and that of TiO_2

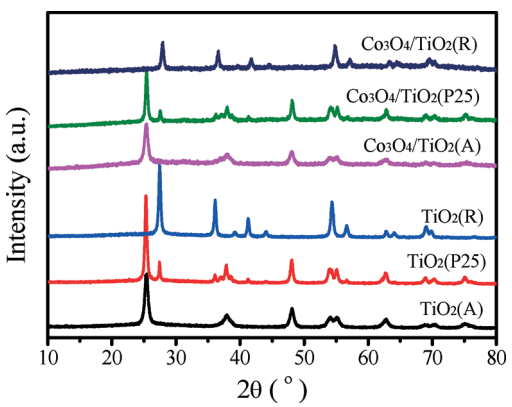

Fig. 3 XRD patterns of the Co_3O_4/TiO_2 catalysts and the TiO_2 supports.

Table 1 The BET surface area (S_{BET}), crystal size and T_{100} values of the catalysts

Catalyst	S_{BET} ($m^2\ g^{-1}$)	Crystal size (nm)	T_{100} (°C)
Co_3O_4/TiO_2 (A)	91.8	15.60	−43
Co_3O_4/TiO_2 (P25)	48.7	20.02 (A), 20.39 (R)	−2
Co_3O_4/TiO_2 (R)	38.0	22.88	45

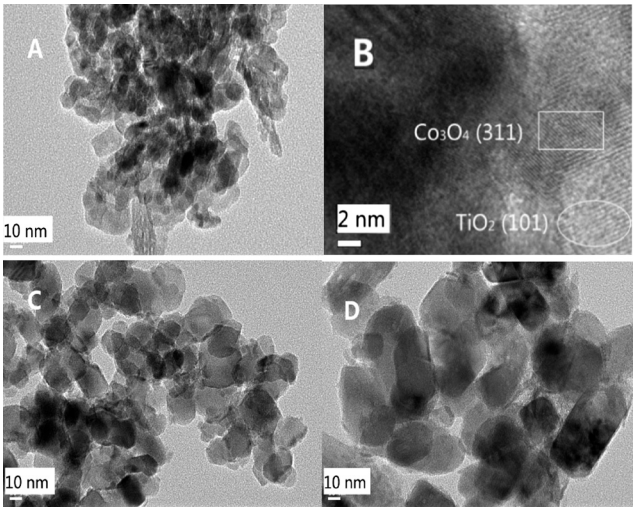

Fig. 4 HR-TEM images of (A and B) Co_3O_4/TiO_2 (A), (C) Co_3O_4/TiO_2 (P25) and (D) Co_3O_4/TiO_2 (R) catalysts.

supports are shown in Fig. 5B. The signals of g values less than 2 were assigned to Ti^{3+} ($3d^1$).[17,29,30] Ti^{3+} species are produced by the trapping of electrons at defective sites in TiO_2.[31] The signals for $g_\perp$ = 1.996 and $g_{||}$ = 1.966 can be attributed to electrons trapped in Ti^{3+} sites.[25,32] As can be observed, the EPR signal of Ti^{3+} can be found on Co_3O_4/TiO_2 (A) and TiO_2 (A) support, and their EPR spectra are almost the same, indicating that Ti^{3+} exists in TiO_2 (A) and after Co_3O_4 loading it still maintained. Comparing with Co_3O_4/TiO_2 (A),

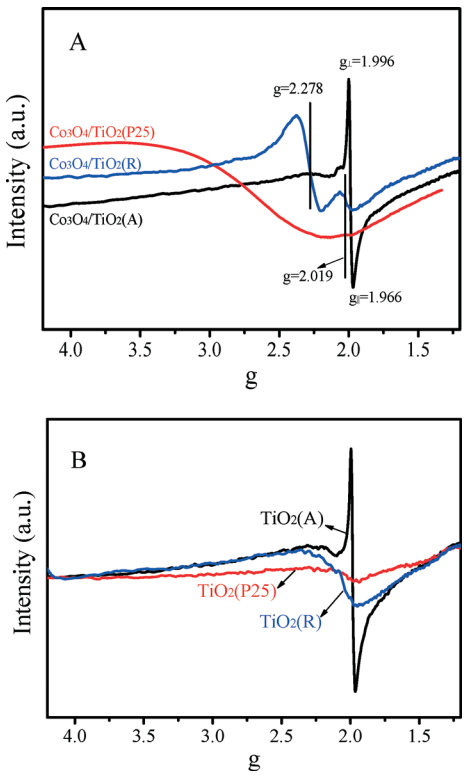

Fig. 5 EPR spectra of the Co_3O_4/TiO_2 catalysts (A) and the TiO_2 supports (B).

and the Ti^{3+} signals on Co_3O_4/TiO_2 (P25) and Co_3O_4/TiO_2 (R) are weakened and broadened, which are contributed to the formation of diamagnetically coupled Ti^{3+} pairs or the coupling of no-diamagnetic Ti^{3+} ions.[33] For TiO_2 (R), its EPR signal is obviously increased after Co_3O_4 loading, and Ti^{3+} ions in Co_3O_4/TiO_2 (R) tend to coupling. As for TiO_2 (P25) or Co_3O_4/TiO_2 (P25), both the EPR signals are very weak and broad, which can be attributed to the structure complexity of the catalyst or a mixture of anatase and rutile TiO_2.

It was reported that the g values in the EPR spectra of TiO_2 are usually bellow 2.1,[29–34] and a resonance at g = 1.979 is characteristic of electrons trapped in tetrahedral Ti^{4+} sites in rutile TiO_2.[34] In the EPR spectrum of Co_3O_4/TiO_2 (R), the signal at g = 2.019 is probably caused by the interaction between Co_3O_4 and TiO_2 (R), and the resonance at g = 2.278 is caused by the widening of the peak, relating to the relaxation time of spin transition. The formation of Ti^{3+} ions can be assumed to represent an unstable state, which can have a significant influence on the crystalline and interfacial region of TiO_2 between deposited Co_3O_4 and TiO_2 support. The strong signal of Ti^{3+} in Co_3O_4/TiO_2 (A) indicates that the catalyst contains a defective structure, which promotes the catalytic performance of Co_3O_4/TiO_2 (A) for CO oxidation.

3.5 Laser Raman spectroscopy

Fig. 6 shows the laser Raman spectra of the TiO_2 supports and Co_3O_4/TiO_2 catalysts. The results show that the vibration bands of anatase TiO_2 are located at 142, 197, 396, 516, and 639 cm^{-1},[35–37] and the vibration bands of rutile TiO_2 are located at 236, 447, and 610 cm^{-1}.[38,39] In the Raman spectrum of TiO_2 (P25), there are the vibration bands of anatase and rutile TiO_2. After Co_3O_4 loading, the Raman vibration bands of TiO_2 are broadened, which may be attributed to an interaction of TiO_2 with cobalt species and disorder in the oxygen sublattice.[40] It was reported that there are some vibration bands at 193, 475, 516, 615, and 680 cm^{-1} in the Raman spectra of Co_3O_4,[35–37,41] in which the band around 680 cm^{-1} is attributed to the A_{1g} symmetry.[42] The vibration band of A_{1g} on Co_3O_4/TiO_2 (A) appeared at 679 cm^{-1}, the lowest wavenumber among the three catalysts, which is a sensitive

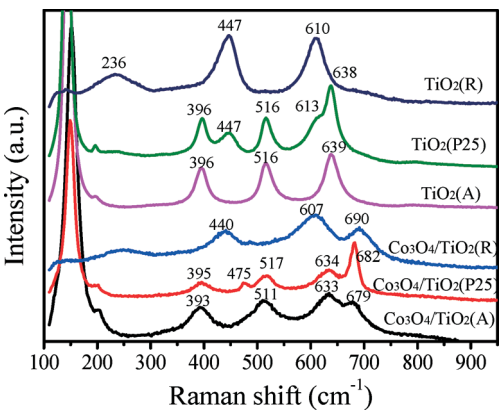

Fig. 6 Laser Raman spectra of the synthesized catalysts and supports.

indication for the highly defective structure.[43] The defective structure is known to play crucial role in the CO oxidation,[44] which may be related to its high catalytic activity. For the Co_3O_4/TiO_2 (P25) catalyst, there are two bands of Co_3O_4 at 475 and 682 cm^{-1}.

3.6 X-ray photoelectron spectroscopy (XPS)

The surface properties of the supported catalysts were further explored by XPS, and the peak-fitting Co 2p XPS spectra of three catalysts are shown in Fig. 7. It was reported that the binding energies of Co^{3+} and Co^{2+} ions are 780.2 ± 0.6 and 781.8 ± 0.6 eV, respectively,[45] and the energy difference between the Co $2p_{3/2}$ peak and the Co $2p_{1/2}$ peak is approximately 15 eV. Two small peaks at 786.3 eV and 804.8 eV are the shake-up satellite peaks of Co^{2+}. The binding energies of Co $2p_{3/2}$ and Co $2p_{1/2}$ of the Co_3O_4/TiO_2 catalysts were summarized in Table 2. The results show that the binding energies of Co 2p in the spectra of Co_3O_4/TiO_2 (A) and Co_3O_4/TiO_2 (P25) are smaller than that of Co_3O_4/TiO_2 (R), indicating that the electron binding ability of Co ions in the Co_3O_4/TiO_2 (R) catalyst is bigger than that in the other two catalysts and the structure nature of TiO_2 support affects the electron transfer ability of Co ions on the TiO_2 support. In addition, we can find that the peak area of Co_3O_4/TiO_2 (R) is the highest among the three catalysts, which might be caused by the lowest surface area of TiO_2 (R). As the Co_3O_4 loading is the same for the three catalysts, the smaller surface area makes the concentration of Co relatively higher.

Fig. 8 shows the O 1s XPS spectra of the three catalysts. The O 1s peak can be fitted to three kinds of Gaussian peaks. The peak at 529.0–530.2 eV (binding energy) should be assigned to surface lattice oxygen (O_{lat}), the peak at 530.3–531.1 eV can be assigned to adsorbed oxygen (O_{ads}, O^-, O_2^- or O_2^{2-}) species, and the peak at 531.6–532.5 eV is commonly ascribed to adsorbed H_2O or surface carbonate.[46–48] The adsorbed oxygen species of O^- and O_2^- are known to be active for oxygen exchange and CO oxidation.[49–51] The results in Fig. 8 show that the O_{ads} peak gradually shifted to higher binding energy from Co_3O_4/TiO_2 (A) to Co_3O_4/TiO_2 (R), indicating that the electronic density of oxygen is decreased, which may be attributed to the contribution of surface hydroxyl groups bounded to the cobalt or titanium ions. The peak of surface hydroxyl and carbonate on Co_3O_4/TiO_2 (R) is much stronger than that on the other two catalysts, resulting in blocking of the active sites for CO adsorption, which is usually considered as a deactivation reason of the catalysts for CO oxidation.[52,53] Therefore, the surface of Co_3O_4/TiO_2 (R) is easily covered by carbonate and hydroxyl groups, resulting in a decrease in its catalytic activity, which can be further verified by the O 1s peak of surface carbonate at 532.4 eV. The ratios of O_{ads}/O_{lat} in Table 2 show that Co_3O_4/TiO_2 (A) with O_{ads}/O_{lat} = 0.58 exhibits the highest activity, and Co_3O_4/TiO_2 (A) with O_{ads}/O_{lat} = 0.72 shows the lowest activity, which should be ascribed to the presence of carbonates on Co_3O_4/TiO_2 (A) to inhibit adsorption of CO on the catalyst surface. The results above show that a relatively clean surface with more adsorbed oxygen is beneficial to improve the catalytic activity of the Co_3O_4/TiO_2 catalyst for CO oxidation.

In the Ti 2p XPS spectra in Fig. 9, the peaks of Ti $2p_{3/2}$ and Ti $2p_{1/2}$ are located at 458.6 and 464.4 eV respectively,

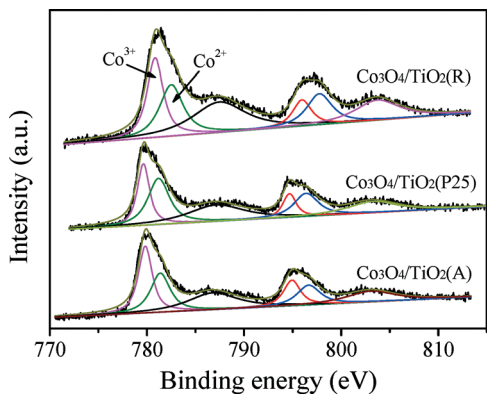

Fig. 7 The Co 2p XPS spectra of Co_3O_4/TiO_2 catalysts.

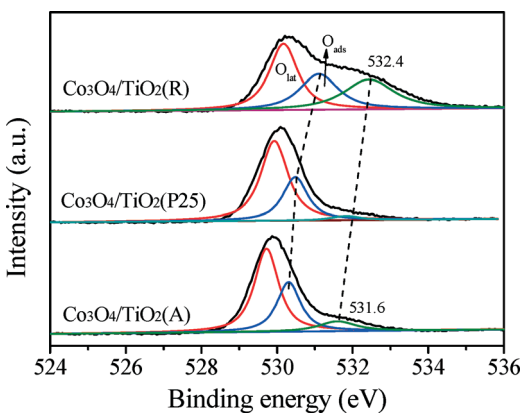

Fig. 8 The O 1s XPS spectra of Co_3O_4/TiO_2 catalysts.

Table 2 XPS data binding energies of Co $2p_{3/2}$, Co $2p_{1/2}$ and O 1s, O_{ads}/O_{lat} of Co_3O_4/TiO_2 (A), Co_3O_4/TiO_2 (P25) and Co_3O_4/TiO_2 (R)

Catalyst	Co $2p_{3/2}$ (eV)	Co $2p_{1/2}$ (eV)	O 1s (eV)	O_{ads}/O_{lat}	Ti $2p_{3/2}$ (eV)	Ti $2p_{1/2}$ (eV)
Co_3O_4/TiO_2 (A)	779.8 781.4	794.9 796.6	529.7 530.3 531.6	0.58	458.6	464.4
Co_3O_4/TiO_2 (P25)	779.6 781.2	794.7 796.4	529.9 530.5 531.8	0.49	458.9	464.7
Co_3O_4/TiO_2 (R)	780.8 782.5	795.9 797.7	530.2 531.1 532.4	0.72	458.9	464.7

which agree well with the values reported.[54] As can be observed, the peak intensity of Co_3O_4/TiO_2 (R) is much lower than that of the other two catalysts, which may be caused by its lower surface area. The Ti 2p peaks of Co_3O_4/TiO_2 (P25) and Co_3O_4/TiO_2 (R) shift to higher binding energy than Co_3O_4/TiO_2 (A), indicating that Ti ions in Co_3O_4/TiO_2 (P25) and Co_3O_4/TiO_2 (R) possess a higher valence state than that in Co_3O_4/TiO_2 (R). The binding energies of Ti 2p are listed in Table 2.

3.7. H_2-TPR

The H_2-TPR profiles of the Co_3O_4/TiO_2 catalysts and TiO_2 supports are shown in Fig. 10. The results show that the TiO_2 supports exhibit weak reduction peaks, so that the reduction peaks of the Co_3O_4/TiO_2 catalysts mainly result from the reduction of Co_3O_4. Co_3O_4/TiO_2 (A) exhibit two reduction peaks at ~297 °C and 445 °C. The peak at 200–350 °C may be attributed to the reduction of Co^{3+} to Co^{2+}, and the peak at 350–700 °C can be attributed to the reduction of Co^{2+} to Co^0.[55,56] For the Co_3O_4/TiO_2 (P25) catalyst, its TPR reduction peaks are similar to that of the Co_3O_4/TiO_2 (A) catalyst, except for the small peak at 325 °C. However, the reason for the reduction peak formation at 325 °C is unclear, and it may be the reduction of Co^{3+} at the interfacial region between anatase and rutile TiO_2. Unlike the TPR curves of Co_3O_4/TiO_2 (A) and Co_3O_4/TiO_2 (P25), the high-temperature reduction peak of Co_3O_4/TiO_2 (R) shifts ~575 °C. Thus Co^{2+} on anatase TiO_2 is easily reduced compared with Co^{2+} on rutile TiO_2. That is to say, the reducibility of Co_3O_4 (special for Co^{2+}) is obviously affected by the structure of the TiO_2 support. Anatase TiO_2 supported Co_3O_4 catalysts show the best reducibility, which results probably in its high catalytic performance for CO oxidation.

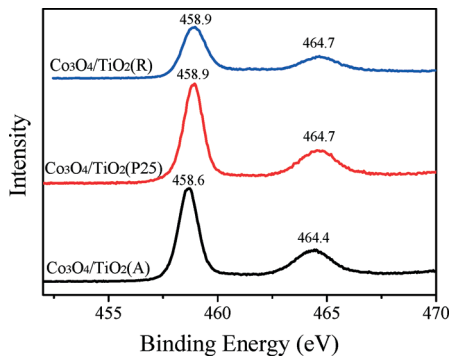

Fig. 9 The Ti 2p XPS spectra of Co_3O_4/TiO_2 catalysts.

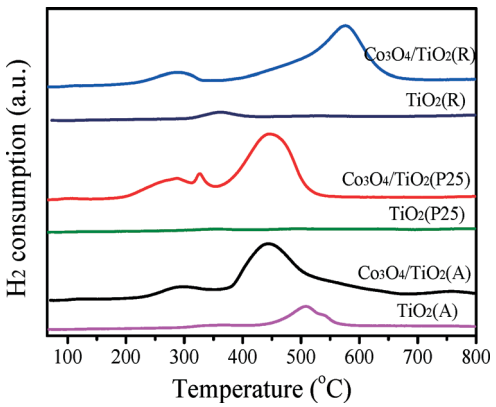

Fig. 10 H_2-TPR profiles of the Co_3O_4/TiO_2 catalysts and TiO_2 supports.

3.8. Discussion

For supported catalysts, the type of support often plays a crucial role in the performance of the catalysts with the help of an interaction between the active components and the support. TiO_2 has three main crystalline structures: anatase (tetragonal *I*4/*amd*), brookite (orthorhombic *Pcab*), and rutile (tetragonal *P*42/*mnm*), and anatase and rutile are usually used as catalyst supports, among them, anatase tends to be more stable at low temperature and rutile is the stable form at higher temperature. And the reactivity of anatase is higher than rutile. Nanba *et al.*[26] found that the TiO_2 crystal phase could affect the oxidation state of Ag supported on TiO_2 catalyst for acrylonitrile decomposition, that is Ag particles on anatase TiO_2 was of an oxidized state and that on rutile was metallic. Kang *et al.*[57] investigated CO oxidation over CuO/TiO_2, and found that CuO dispersion, an interaction between CuO and TiO_2 and the oxidation state of copper component were changed by the crystal structure of the TiO_2 support, and the catalytic activity of the catalyst supported on rutile TiO_2 was the highest. For different reactions with different catalysts, the effect of the crystal phase of TiO_2 on the catalytic performance might not be the same. Herein, the CO oxidation over Co_3O_4/TiO_2 was investigated, and the effect of the crystal phase of TiO_2 on the catalytic performance of Co_3O_4 catalyst was discussed.

The Co_3O_4/TiO_2 (A) catalyst exhibits higher activity and better stability for CO oxidation than Co_3O_4/TiO_2 (P25) and Co_3O_4/TiO_2 (R) (Fig. 1 and 2), which may be attributed to the following reasons. (1) The Co_3O_4/TiO_2 (A) catalyst possesses a higher BET surface area and smaller crystalline size than the other two catalysts. As the diffraction peaks of Co_3O_4 cannot be detected in the XRD profiles (Fig. 3), Co_3O_4 is highly dispersed on the TiO_2 support and interacts closely with the support. (2) The EPR results (Fig. 5) indicate that Ti^{3+} species only exists in Co_3O_4/TiO_2 (A), which is in an unstable state and has a significant influence on the catalytic property of the catalyst. (3) In the Raman spectra (Fig. 6), the A_{1g} peak of Co_3O_4 shifted to lower wavenumber when anatase TiO_2 was used as the support, which illustrates a highly defective structure for Co_3O_4/TiO_2 (A) and plays a crucial role in the CO oxidation. (4) The electron transfer ability of Co ions was enhanced by the help of the anatase TiO_2 support, resulting in a good oxygen adsorption ability of Co_3O_4/TiO_2 (A) by means of the clean surface, which were verified by the XPS results (Fig. 7 and 8). (5) The H_2 reduction behaviour of Co_3O_4 is improved due to the presence of the anatase TiO_2 support (Fig. 10), unlike Co_3O_4/TiO_2 (R) and Co_3O_4/TiO_2 (P25).

The results above show that the physicochemical properties of Co_3O_4 can be varied by the crystal structure of the

TiO_2 support. The presence of Ti^{3+} ions in Co_3O_4/TiO_2 (A) as a defective structure, is in favour of forming oxygen vacancies,[58] which was observed in Raman spectra (Fig. 6). The oxygen vacancies can adsorb oxygen from the gas phase and weaken its bond to form the activated oxygen species.[59] The activated oxygen species could accelerate the oxygen exchange and surface diffusion to promote the catalytic oxidation of CO. In other words, the defective structure can accelerate the oxygen exchange and surface diffusion to prevent the formation of carbonate species and slow down the accumulation of carbonate species, resulting in an increase in the catalytic activity for CO oxidation, which was verified by the O 1s XPS spectra (Fig. 8), because the accumulation of carbonate species on the surface would lead to the decrease of the catalytic activity for CO oxidation.[52,53]

Furthermore, the reducibility of Co_3O_4 is also affected by the crystalline structure of the TiO_2 support, and the reduction temperature of Co_3O_4/TiO_2 (A) is lower compared with the other two catalysts. In the process of CO oxidation, the reduction of Co ions is a very important step in the redox catalytic cycle, which plays a crucial role in the CO oxidation.

4. Conclusions

Highly dispersed Co_3O_4 nanoparticles supported on three types of TiO_2 with different crystalline structures (anatase phase TiO_2 (A), P25 (Degussa) and rutile phase TiO_2 (R)) were prepared by a deposition–precipitation method. The results show that the crystalline structure of TiO_2 would affect obviously the physicochemical and catalytic properties of the Co_3O_4/TiO_2 catalysts, and the Co_3O_4/TiO_2 (A) catalyst exhibits the highest activity for CO oxidation among the three Co_3O_4/TiO_2 catalysts. The excellent catalytic performance of the Co_3O_4/TiO_2 (A) catalyst for CO oxidation can be attributed to the following reasons:

(1) The Co_3O_4/TiO_2 (A) catalyst possesses a higher BET surface area and smaller crystalline size than Co_3O_4/TiO_2 (P25) and Co_3O_4/TiO_2 (R); and Co_3O_4 is highly dispersed on the TiO_2 support and interacts closely with the support.

(2) The Ti^{3+} species exists in Co_3O_4/TiO_2 (A), which is in an unstable state and has a significant influence on the catalytic property of the catalyst. Furthermore Co_3O_4/TiO_2 (A) exhibits a highly defective structure that plays a crucial role in the CO oxidation.

(3) The electron transfer ability of Co ions was enhanced by the help of the anatase TiO_2 support, resulting in a good oxygen adsorption ability of Co_3O_4/TiO_2 (A) by means of the clean surface. The reducibility of Co_3O_4 is improved due to the presence of the anatase TiO_2 support, so that Co_3O_4/TiO_2 (A) possesses the best redox property among the three Co_3O_4/TiO_2 catalysts.

Acknowledgements

This project was financially supported by National Natural Science Foundation of China (21273150), the National Basic Research Program of China (2010CB732300, 2013CB933201), the national high technology research and development program of China (2011AA03A406, 2012AA062703), the Fundamental Research Funds for the Central Universities, the "ShuGuang" Project (10GG23) of Shanghai Municipal Education Commission.

Notes and references

1 M. Shelef and R. W. McCabe, *Catal. Today*, 2000, **62**, 35.
2 M. V. Twigg, *Appl. Catal., B*, 2007, **70**, 2.
3 Y. X. Shen, G. Z. Lu, Y. Guo and Y. Q. Wang, *Chem. Commun.*, 2010, **46**, 8433.
4 A. Saramat, P. Thormählena, M. Skoglundha, G. S. Attard and A. E. C. Palmqvist, *J. Catal.*, 2008, **253**, 253.
5 N. Lopez, T. V. W. Janssens, B. S. Clausen, Y. Xu, M. Mavrikakis, T. Bligaard and J. K. Nørskov, *J. Catal.*, 2004, **223**, 232.
6 M. Haruta, T. Kobayashi, H. Sano and N. Yamada, *Chem. Lett.*, 1987, **16**, 405.
7 J. Jansson, *J. Catal.*, 2000, **194**, 55.
8 J. Jansson, A. E. C. Palmqvist, E. Fridell, M. Skoglundh, L. O. Sterlund, P. Thormahlen and V. Langer, *J. Catal.*, 2002, **211**, 387.
9 H. K. Lin, C. B. Wang, H. C. Chiu and S. H. Chien, *Catal. Lett.*, 2003, **86**, 63.
10 H. K. Lin, H. C. Chiu, H. C. Tsai, S. H. Chien and C. B. Wang, *Catal. Lett.*, 2003, **88**, 169.
11 D. A. H. Cunningham, T. Kobayashi, N. Kamijo and M. Haruta, *Catal. Lett.*, 1994, **25**, 257.
12 P. Thormählen, M. Skoglundh, E. Fridell and B. Andersson, *J. Catal.*, 1999, **188**, 300.
13 Y. Z. Wang, Y. X. Zhao, C. G. Gao and D. S. Liu, *Catal. Lett.*, 2007, **116**, 136.
14 X. W. Xie, Y. Li, Z. Q. Liu, M. Haruta and W. J. Shen, *Nature*, 2009, **458**, 746.
15 J. Li, G. Z. Lu, G. S. Wu, D. S. Mao, Y. Q. Wang and Y. Guo, *Catal. Sci. Technol.*, 2012, **2**, 1865.
16 J. Li, G. Z. Lu, G. S. Wu, D. S. Mao, Y. L. Guo, Y. Q. Wang and Y. Guo, *RSC Adv.*, 2013, **3**, 12409.
17 J. Panpranot, K. Kontapakdee and P. Praserthdam, *J. Phys. Chem. B*, 2006, **110**, 8019.
18 P. Weerachawanasak, O. Mekasuwandumrong, M. Arai, S. I. Fujita, P. Praserthdam and J. Panpranot, *J. Catal.*, 2009, **262**, 199.
19 P. Castillo-Villalón and J. Ramírez, *J. Catal.*, 2009, **268**, 39.
20 F. Cárdenas-Lizana, S. Gómez-Quero, H. Idriss and M. A. Keane, *J. Catal.*, 2009, **268**, 223.
21 C. H. Lin, J. H. Chao, C. H. Liu, J. C. Chang and F. C. Wang, *Langmuir*, 2008, **24**, 9907.
22 G. Li, N. M. Dimitrijevic, L. Chen, T. Rajh and K. A. Gray, *J. Phys. Chem. C*, 2008, **112**, 19040.
23 L. G. Devi, N. Kottam and S. G. Kumar, *J. Phys. Chem. C*, 2009, **113**, 15593.
24 B. Ohtani, O. O. P. Mahaney, F. Amano, N. Murakami and R. Abe, *J. Adv. Oxid. Technol.*, 2010, **13**, 247.

25 Y. Li, B. Xu, Y. Fan, N. Feng, A. Qiu, J. W. Miao, J. He, H. Yang and Y. Chen, *J. Mol. Catal. A: Chem.*, 2004, **216**, 107.
26 T. Nanba, S. Masukawa, J. Uchisawa and A. Obuchi, *Appl. Catal., A*, 2012, **419–420**, 49.
27 H. Iida and A. Igarashi, *Appl. Catal., A*, 2006, **298**, 152.
28 A. Patterson, *Phys. Rev.*, 1939, **56**, 978.
29 J. C. Conesa, P. Malet, G. M. Unuera, J. Sanz and J. Soria, *J. Phys. Chem.*, 1984, **88**, 2986.
30 T. M. Salama, H. Hattorl, H. Kita, K. Ebitani and T. Tanaka, *J. Chem. Soc., Faraday Trans.*, 1993, **89**, 2067.
31 S. Ikeda, N. Sugiyama, S. Y. Murakami, H. Kominami, Y. Kera, H. Noguchi, K. Uosaki, T. Torimoto and B. Ohtani, *Phys. Chem. Chem. Phys.*, 2003, **5**, 778.
32 L. Bonneviot and G. L. Haller, *J. Catal.*, 1988, **113**, 96.
33 P. Claus, S. Schimpt, R. Schodel, P. Kraak, W. Morke and D. Honicke, *Appl. Catal., A*, 1997, **165**, 429.
34 G. H. Li, N. M. Dimitrijevic, L. Chen, J. M. Nichols, T. Rajh and K. A. Gray, *J. Am. Chem. Soc.*, 2008, **130**, 5402.
35 T. Xiao, S. J. Ji, H. Wang, K. S. Coleman and M. L. H. Green, *J. Mol. Catal. A: Chem.*, 2001, **175**, 111.
36 Y. Brik, M. Kacimi, M. Ziyad and F. Bozon-Verduraz, *J. Catal.*, 2001, **202**, 118.
37 Y. Brik, M. Kacimi, F. Bozon-Verduraz and M. Ziyad, *J. Catal.*, 2002, **211**, 470.
38 M. S. Wainwright and N. R. Foster, *Catat. Rev.-Sci. Eng.*, 1979, **19**, 211.
39 M. Wu, W. Zhang, Z. Du and Y. Huang, *Mod. Phys. Lett. B*, 1999, **13**, 167.
40 J. Cai, C. Raptis, Y. S. Raptis and E. Anastassakis, *Phys. Rev. B: Condens. Matter*, 1995, **51**, 201.
41 H. Ohtsuka, T. Tabata, O. Okada, L. M. F. Sabatino and G. Bellussi, *Catal. Lett.*, 1997, **44**, 265.
42 J. Jiang and L. C. Li, *Mater. Lett.*, 2007, **61**, 4894.
43 Q. Liu, L. C. Wang, M. Chen, Y. Cao, H. Y. He and K. N. Fan, *J. Catal.*, 2009, **263**, 104.
44 H. Y. Li, H. F. Wang, Y. L. Guo, G. Z. Lu and P. Hu, *Chem. Commun.*, 2011, **47**, 6105.
45 M. Kang, M. W. Song and C. H. Lee, *Appl. Catal., A*, 2003, **251**, 143.
46 A. F. Carley, M. W. Roberts and A. K. Santra, *J. Phys. Chem. B*, 1997, **101**, 9978.
47 N. Yamazoe, Y. Teraoka and T. Seiyama, *Chem. Lett.*, 1981, 1767.
48 J. L. G. Fierro and L. G. Tejuca, *Appl. Surf. Sci.*, 1987, **27**, 453.
49 C. Naccache, P. Meriaudeau and M. Che, *Trans. Faraday Soc.*, 1971, **67**, 506.
50 V. A. Shvets and V. B. Kazansky, *J. Catal.*, 1972, **25**, 123.
51 M. Che and A. J. Tench, *Adv. Catal.*, 1983, **32**, 1.
52 Y. Denkwitz, A. Karpenko, V. Plzak, R. Leppelt, B. Schumacher and R. J. Behm, *J. Catal.*, 2007, **246**, 74.
53 J. Jansson, M. Skoglundh, E. Fridell and P. Thormählen, *Top. Catal.*, 2001, **16/17**, 385.
54 B. M. Reddy, B. Chowdhury, I. Ganesh, E. P. Reddy, T. C. Rojas and A. Fernandez, *J. Phys. Chem. B*, 1998, **102**, 10176.
55 Y. Y. Liu, T. Hanaoka, T. Miyazawa, K. Murata, K. Okabe and K. Sakanishi, *Fuel Process. Technol.*, 2009, **90**, 901.
56 D. Shanke, S. Vada, E. A. Blekkan, A. M. Hilmen, A. Hoff and A. Holmen, *J. Catal.*, 1995, **156**, 85.
57 M. Y. Kang, H. J. Yun, S. J. Yu, W. Kim, N. D. Kim and J. Yi, *J. Mol. Catal. A: Chem.*, 2013, **368–369**, 72.
58 K. Suriye, P. Praserthdam and B. Jongsomjit, *Appl. Surf. Sci.*, 2007, **253**, 3849.
59 Z. P. Hao, D. Y. Cheng, Y. Guo and Y. H. Liang, *Appl. Catal., B*, 2001, **33**, 217.